Simulink Model for Hybrid Power System Test-bed

M. C. Knauff, *Student Member, IEEE*, C. J. Dafis, *Member, IEEE*, D. Niebur, *Member, IEEE*, H. G. Kwatny, *Life Fellow, IEEE*, C. O. Nwankpa, *Senior Member, IEEE, and J. Metzer*

***Abstract*—The Hybrid Power System Test-bed currently being constructed at NAVSEA Philadelphia is designed to serve as a developmental platform for the evaluation of hybrid power and propulsion options related to unmanned surface vehicles (USVs). Prior to component integration, a Matlab/Simulink model of the test-bed was created to simulate the system interactions and assist in the detailed electrical design. A reduced order system model was required before a detailed analysis of the individual components was performed. This paper describes the evolution of the test-bed model and the work to date in developing detailed component models for the system.**

***Index Terms*—unmanned surface vehicles, hybrid power systems, modeling and simulation.**

I. Introduction

DUE to the various operating characteristics that proposed Unmanned Surface Vehicles (USVs) possess, various propulsion and electrical distribution technologies need to be integrated. Systems incorporating batteries, fuel cells and diesel engines have been envisioned, and the proper size and placement of these components is of interest. The Hybrid Power System Test-bed is a proposed configuration of sources, loads, and power electronic devices providing a variety of options that currently are being assembled in a small-scale hardware demonstration at NAVSEA Philadelphia. The primary purpose of this test-bed is to facilitate the design of power system architectures for USVs using various system configuration options, and also to serve as a platform to evaluate system level power management schemes currently under development [1].

To determine the operating conditions and constraints of the physical system, a system simulation of the test-bed was constructed to facilitate the detailed electrical system design. The Matlab Simulink environment was selected utilizing the available models in the SimPowerSystems Blockset.

This paper is organized as follows. Section II describes the various devices included in the test-bed. In section III the strategy used to develop the test-bed model is discussed. The initial modeling and subsequent updating of the battery model is discussed in section IV. Section V and VI present results obtained from the individual models and the overall system respectively. Finally, section VII concludes the paper.

Manuscript received March 5, 2007. This work was supported in part by the Office of Naval Research Contract Number N00014-14-04-M-0285 and the NSF-Navy Civilian Service (NNCS) Fellowship-Scholarship Program.

M.C. Knauff, D. Niebur, H. G. Kwatny, and C. O. Nwankpa are with the Drexel University, Philadelphia, PA 19104 USA (e-mail: mck39@ drexel.edu, [Niebur, Kwatny, Nwankpa]@coe.drexel.edu).

C. J. Dafis and J. Metzer are with NAVSEA-Philadelphia, Philadelphia, PA 19112 USA (e-mail: dafiscj@nswccd.navy.mil).

II. Device Descriptions

One potential configuration of the test-bed is depicted in Fig. 1 (measurement related blocks have been removed). Generally, the test-bed consists of two main sources and two loads, connected via a DC bus. The generation components consist of a diesel generator set and: a Lithium-Ion (Li-Ion) battery pack, and the load components consist of, a programmable load and a permanent magnet rim-driven motor serving as a propulsion motor that is submerged in a tank,. Each source is connected to the DC bus via a power electronic converter.

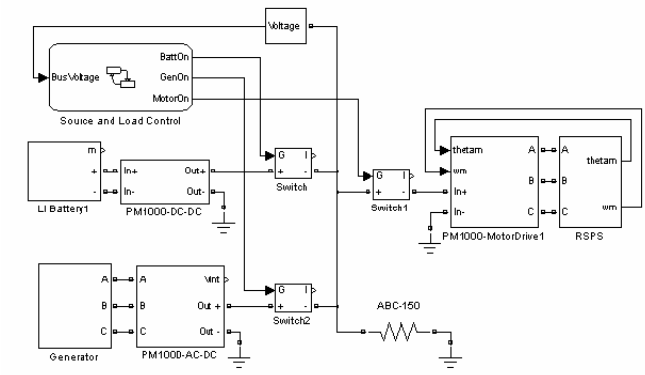

Fig. 1. Simulink model of test-bed. (Note: measurement blocks not included.)

The diesel generator set used in the test-bed is the Caterpillar Olympian D80-4, providing 75kW, 3-phase 60Hz 120/208V power. A list of the generator parameters is provided in Table 1.

TABLE I
GENERATOR PARAMETERS

Xd	3.82	Xo	0.005
Xd'	0.15	Td'	100ms
Xd"	0.089	Td"	10ms
Xq	2.29	Tdo'	2555ms
Xq"	0.110	Ta	15ms
X2	0.1		

The Lithium-Ion (Li-Ion) battery used was custom built by Lithium Technology Corporation. The battery consists of 33 cells providing between 3 and 4 volts each for a total voltage

of approximately 120 V. The capacity of the battery is estimated at 60 Ah. Other than these electrical operation characteristics, no specific parameter values associated with a battery model were provided regarding for example transient behavior or state of charge vs. open circuit voltage curves. Therefore, tests were performed to extract these parameters and build an adequate simulation model of the battery.

The rim-driven motor is an experimental in-house design of an electric propulsion motor producing low levels of acoustic noise. This motor was initially designed to validate motor design principles that can be applied to a podded Secondary Propulsion Unit for submarines. For the initial system simulation, the model of this motor is approximated with a generic permanent magnet motor that will further be developed in the future to reflect the inherent motor design features.

The resistor element shown in the lower right of Fig. 1. represents the Aerovironment ABC-150 power processing system. This component is capable of emulating a broad range of devices such as motors, electronic equipment, faults, and resistive loads, and will be utilized as a load emulator in the test-bed. Currently, a simplified resistive model and constant power model are being used to depict the ABC-150 until the unit is rigorously tested and its associated parameters are extracted.

The last components are three power electronic converters used in the test-bed. They include an AC-DC converter, a DC-DC converter, and the motor drive for the RSPS. Each of these devices is constructed as a combination of one or more Power Electronic Building Blocks (PEBBs) [2, 3], and in particular, the American Superconductor PM1000 Power module concept has been used. These devices can be configured in a variety of ways to accommodate various applications. Similar to the rim-driven motor, these components are being tested to extract the specific model parameters, and are currently being simulated using generic power electronic models with custom control algorithms.

III. Model Development Strategy

The basic concept behind this strategy was to first model the system in a manner that a) took into account all known parameters of the devices, b) ensured that each device behaved in a manner reflective of typical behavior of similar devices, and c) led to adequate performance and stability of the overall system. The goal initially was to provide a system level model that can assist in the detailed electrical design of the system providing feedback into the transient characteristics to properly size system cabling and protection elements.

After this initial model was constructed the individual system component models are updated to reflect the specific components of the system. Upon delivery of these components, tests are conducted to extract the specific component parameters and update the simulation model. First the individual component model is changed to match experimental data. This component model is then placed in the system model, to ensure the interactions with the other system components are acceptable. Again adjustments are made on the remaining devices to ensure adequate performance and stability.

At present this process is still on-going and the detailed models for the rim-driven motor, ABC-150 power processing unit and PM1000 power electronic modules are still in an iterative state. The following section provides an overview of the process used to extract these models, focusing on the Li-Ion battery.

IV. Battery Modeling and Revision

While developing the Simulink model for the Li-Ion battery, basic information about the device electrical characteristics was known. The general architecture of the battery was known in advance. The nominal voltage of the battery was designed to be about 120 Volts. To meet this requirement 33 smaller cells each between 3 and 4 volts were used. The capacity of these cells was to be approximately 60 Amp-hours (Ah).

There are many known battery models published in literature. For an overview of the different types of models available refer to [4]. A model proposed in [5] was selected for the test-bed due to its capability in modeling the dynamic and steady state behavior of the battery and due to its relative simplicity. The circuit diagram of the model published in [5] is shown in Fig. 2. The battery model is described by two circuit diagrams which interact via a nonlinear voltage controlled voltage source and a current controlled current source. The first circuit consists of a large capacitor which represents the state of charge (SOC) of the battery, while the other circuit consists of two RC circuits and a series resistance. The second circuit models the transient behavior and voltage-current relationship of the battery.

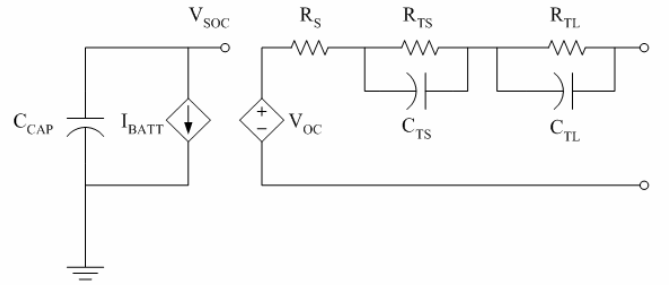

Fig. 2. Circuit diagram for battery model adapted from [5].

To implement this model in Simulink an ordinary differential equation representing the circuit diagram in [5] was derived yielding

$$\dot{\mathbf{x}} = \begin{bmatrix} 0 & 0 & 0 \\ 0 & -(R_{TS}C_{TS})^{-1} & 0 \\ 0 & 0 & -(R_{TL}C_{TL})^{-1} \end{bmatrix} \mathbf{x} + \begin{bmatrix} -C_{CAP}^{-1} \\ -C_{TS}^{-1} \\ -C_{TL}^{-1} \end{bmatrix} \mathbf{u} \qquad (1)$$

$$\mathbf{y} = g(x_1) + x_2 + x_3 + R_s\mathbf{u}$$

where R_{TS} and C_{TS} are the resistance and capacitance in the short transient RC circuit, R_{TL} and C_{TL} are the resistance and capacitance in the long transient RC circuit, C_{CAP} is the capacitance representing the capacitance of the battery, R_S is the

series resistance, g is the non-linear SOC function. The state vector **x** represents the voltage across C_{CAP}, C_{TS}, and C_{TL}. The input **u** is the current entering the battery, and the output **y** is the voltage across the battery terminals.

This equation was then implemented in Simulink using several standard Simulink blocks as well as some of the SimPowerSystems blocks. The nonlinear SOC relationship was implemented using a lookup table with a set of 10 values ranging from full charge to complete discharge.

Most of the other test-bed components were modeled using the SimPowerSystems blockset, which uses a different style connection than is usually used in Simulink. Because the differential equation above was implemented primarily using standard Simulink blocks, an interface had to be setup in the model to link between the two types of connections. The battery model is shown in Fig. 3. On the right hand side of the diagram is the interface, consisting of a current measurement block and a voltage source block.

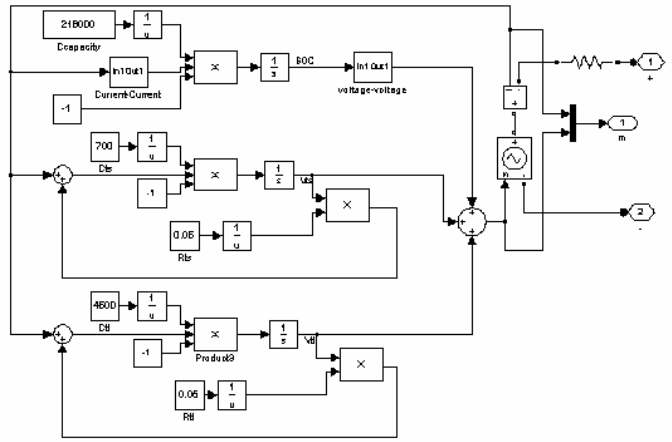

Fig. 3. Simulink model of Li-Ion battery.

The transient behavior, internal non-linear relationship, and internal resistance of the Li-Ion battery were initially unknown. Therefore the parameters for the Polymer Li-Ion battery tested in [5] were used as a basis for the model. However, the nominal voltage had to be increased significantly to match the battery voltage listed in the specification by scaling the internal SOC relationship in the model.

Shortly after completing the Simulink model of the test-bed, the Li-Ion battery arrived at the facility and underwent initial testing. The first available test results were a series of constant resistance full discharges of the battery. The experimental data included the current and voltage at the terminals of the battery as well as several other values pertaining to individual cells, temperature, etc. These test results were sufficient to update the SOC relationship in the model.

To calculate the state of charge, Equation (2) was used. The integral was approximated at each time step by a simple cumulative sum, the error incurred in doing so was negligible considering the large number of data points.

$$v_{SOC}(t) = v_{SOC}(0) - \frac{1}{C_{CAP}} \int_0^t i(\tau) d\tau \qquad (2)$$

$v_{SOC}(t)$ is the internal voltage representing state of charge at time t, and i(t) is the current at time t.

According to the manufacturer, at full charge each cell in the battery should measure 4.2 Volts. However, the test results showed an initial voltage of 4.09 Volts for each cell. To account for this difference, it was assumed that the test began at a 90% state of charge. Therefore $v_{soc}(0)$ was set to 0.9 in the above equation.

Once the SOC throughout the test was determined, the lookup table could easily be updated by searching through the data and referring to the corresponding terminal voltage at different SOC points. The SOC relationship was then computed by accounting for the voltage loss in the resistive elements of the circuit.

Fig. 4. and Fig. 5. compare the initial and refined models of the battery with respect to the experimental data. It is clear from the figures that updating the model has significantly improved its accuracy.

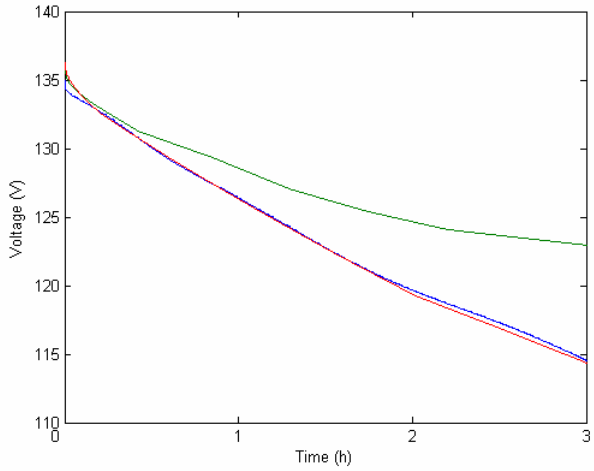

Fig. 4. Comparison of battery voltage for experimental data and initial and refined models.

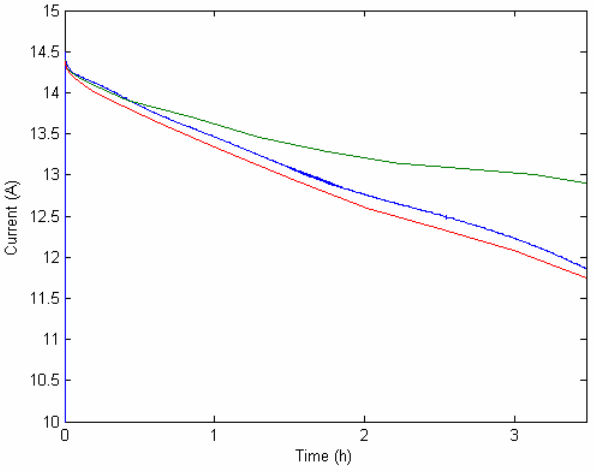

Fig. 5. Comparison of battery current for experimental data and initial and refined models.

V. Summary of Other System Models

Each device in the test-bed was simulated individually. The device models and plots of these simulations are briefly reviewed below.

The parameters of the DC-DC converter included the switching frequency of the converter, the size of the capacitor and inductor, the resistive losses in the inductor, and the proportional and integral gains for the PI controller used to regulate the output voltage. The switches and capacitor in the converter were assumed to be ideal.

The switching frequency of the actual converter is listed in the specification as ranging between 4kHz and 8kHz and therefore 4kHz was chosen for the model's switching frequency. Based on this value the capacitor and inductor were selected to be 226.6 μF and 4.5 mH respectively in order to achieve a reasonably small ripple voltage and input ripple current. The inductor was assumed to have a resistive loss of 0.04 Ω. The proportional and integral gains for the PI controller were selected to be 5 and 0.003 respectively.

This choice in parameters yielded the following performance: 5 % ripple voltage, 6 % input ripple current, 0.146s rise time, 0.190s settling time, and no overshoot at startup. Fig. 6. shows the boost converter at startup.

The AC-DC converter used to connect the generator set to the DC bus consisted of a three phase rectifier feeding a boost converter. The boost converter parameters were chosen identical to those above, and Figs. 7. shows the AC-DC converter at startup.

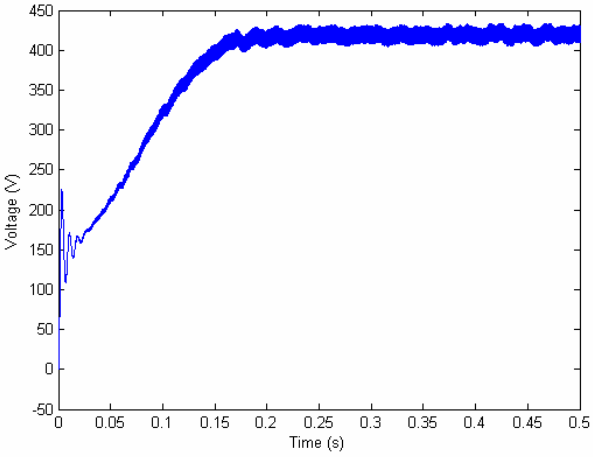

Fig. 6. Boost converter output voltage at startup.

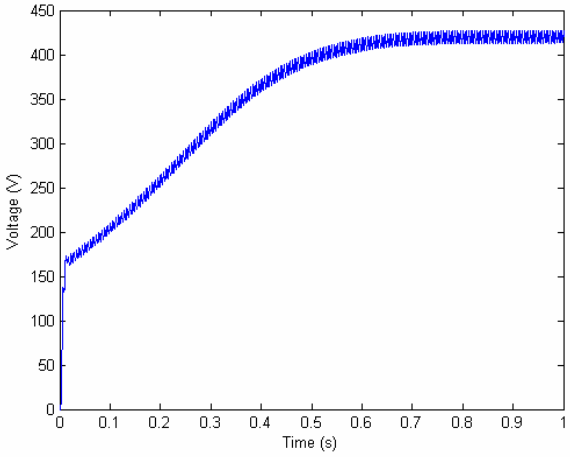

Fig. 7 AC-DC converter output voltage at startup.

The generator set model is shown in Fig. 8. The generator set uses two control loops, one which uses the exciter to regulate the output voltage, and one to regulate the frequency. Although the electrical parameters of the generator were provided by the manufacturer the parameters of the excitation system and the frequency regulator parameters were estimated and will further be refined with additional testing of the diesel generator set. Figs. 9 and 10 show the voltage and frequency of the generator at startup.

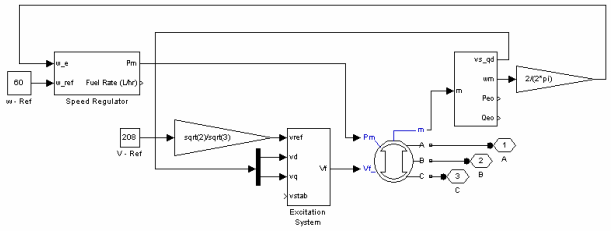

Fig. 8 Generator set model.

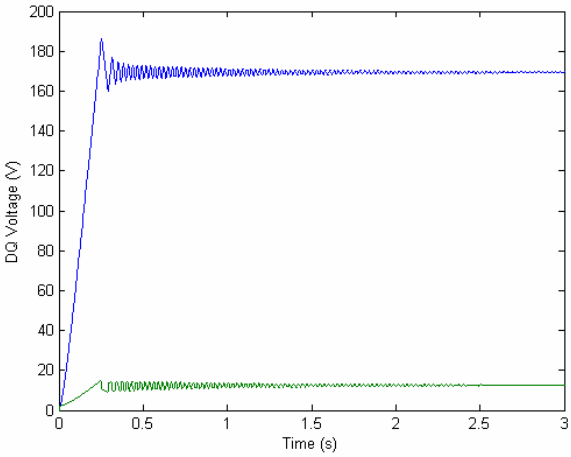

Fig. 9. Generator set stator voltage at startup.

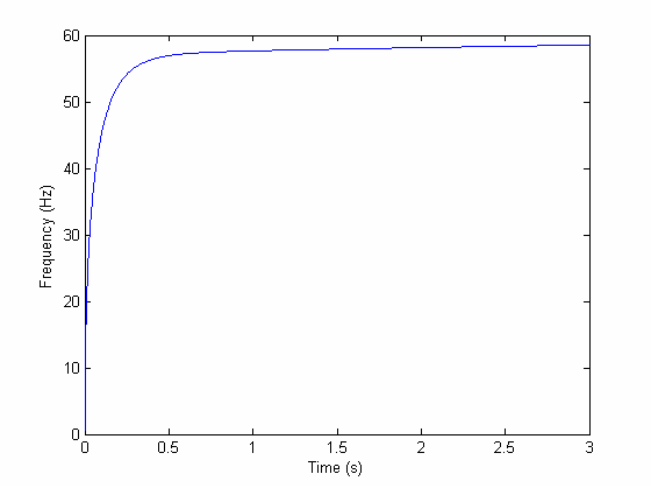

Fig. 10. Generator set frequency at startup.

The rim-driven motor and motor drive models were created together. The parameters of the rim-driven motor are not publicly available, so parameters for the motor were chosen to reflect typical permanent magnet motors in the respective power range.

The motor drive for the propulsion motor consists of three half bridges supplying each phase of the motor. The motor has a hierarchical control structure. The main PI controller supplies three current references for each phase based on the speed and angular position of the motor shaft. Three sub-controllers adjust the pulse width of each half bridge controlling the output current supplied to the motor.

The parameters of each of these controllers were chosen to allow the motor to operate at rated speed. The main controller consisted of a PI controller which was then modulated for each phase. The modulation consisted of a sinusoidal function synchronized with the angular position of the shaft for one phase and shifted by 120° for the remaining two phases. In addition this sinusoidal function was offset by a small phase angle to compensate for the rise time of the half bridge circuits. Fig. 11 shows the effect of this offset.

While it sufficed to use a PI controller for the main controller, the half bridges required an output-feedback controller. The root locus of the half bridge circuits with feedback introduced yielded poles which were either in the right half plane or very close to it depending on the feedback gain. The Matlab SISO Design Toolbox was used to find a compensator which led to a more stable system with improved performance, and typical results are depicted in Figs. 11, 12, and 13.

VI. Overall Results

The purpose of the test-bed is to have a physical system available for use in experiments focusing on integrating multiple sources in a small scale power system. Therefore, it is important to know how the system will behave with either of the two power sources connected to the system.

A stateflow chart was included in the test-bed for future implementation of power management schemes, timed switching, etc. The controller modeled in stateflow controls three switches placed between the DC bus and each power source as well as the motor load. A simple example chart is shown in Fig. 14. The controller connects the battery to the DC bus via one of the switches, waits for the voltage to rise above 410 V and then connects the propulsion motor to the DC bus.

To test the stability and behavior of the overall system the simulated test-bed was operated in two different configurations. One configuration used the generator set as a power source, while the other used the Li-Ion battery. Results showing the bus voltage and the motor speed using the generator set source are shown in Figs 15 and 16 while results using the battery are shown in Figs 17 and 18.

VII. Conclusion

Future work in developing the Simulink model includes the testing and updating of all the remaining pieces of equipment. The generic models can then be replaced in the overall test-bed model. Upon completion of the test-bed, the overall model can be simulated to verify its accuracy.

Acknowledgment

The authors would like to thank Jeffrey McLaughlin for the setup and testing of the Li-Ion battery described above, and for providing the data from these tests.

References

[1] H. G. Kwatny, E. Mensah, D. Niebur, and C. Teolis, "Optimal shipboard power system management via mixed integer dynamic programming," in *IEEE Electric Ship Technologies Symposium*, 2005, pp. 55-62.

[2] T. Ericsen and A. Tucker, "Power Electronics Building Blocks and potential power modulator applications," in *Conference Record of the 1998 Twenty-Third International Power Modulator Symposium*, 1998, pp. 12-15.

[3] T. Ericsen, N. Hingorani, and Y. Khersonsky, "Power electronics and future marine electrical systems," *Industry Applications, IEEE Transactions on,* vol. 42, pp. 155-163, 2006.

[4] P. Singh and A. Nallanchakravarthula, "Fuzzy logic modeling of unmanned surface vehicle (USV) hybrid power system," in *Proc. 2005 Intelligent Systems Application to Power Systems*, p. 7 pp.

[5] M. Chen and G. A. Rincon-Mora, "Accurate electrical battery model capable of predicting runtime and I-V performance," *IEEE Transactions on Energy Conversion,* vol. 21, pp. 504-511, 2006.

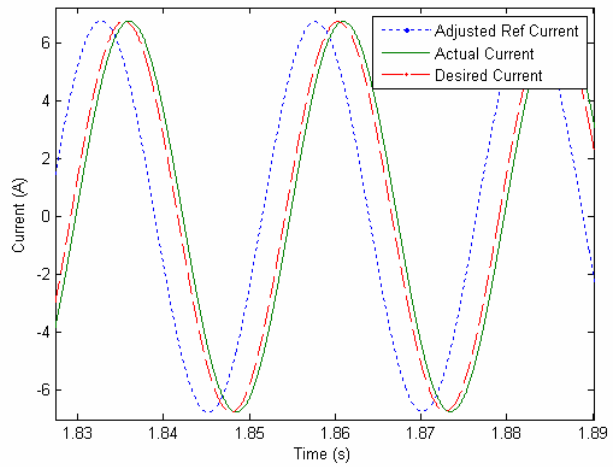

Fig. 11. Comparison of desired current, reference current, and actual current for RSPS motor.

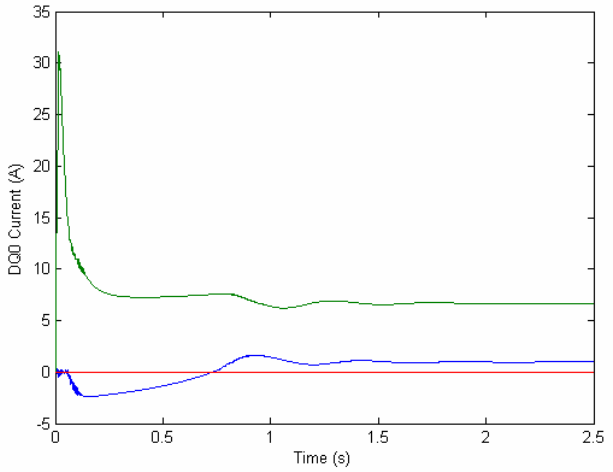

Fig. 12. RSPS DQ0 current at startup.

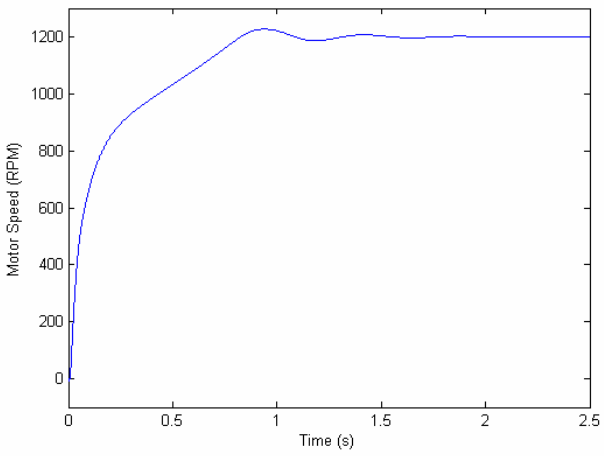

Fig. 13. RSPS speed at startup.

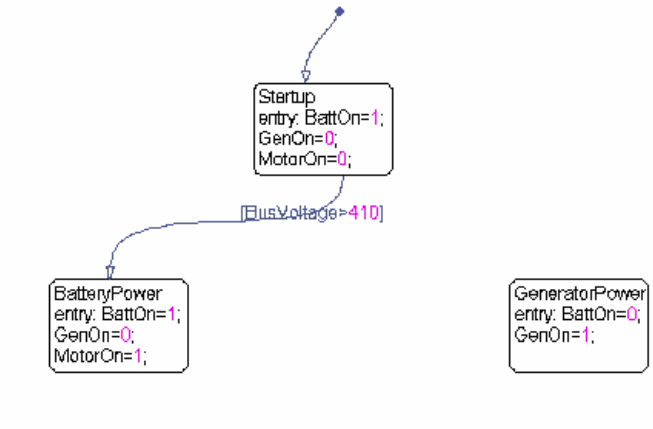

Fig. 14. Stateflow chart.

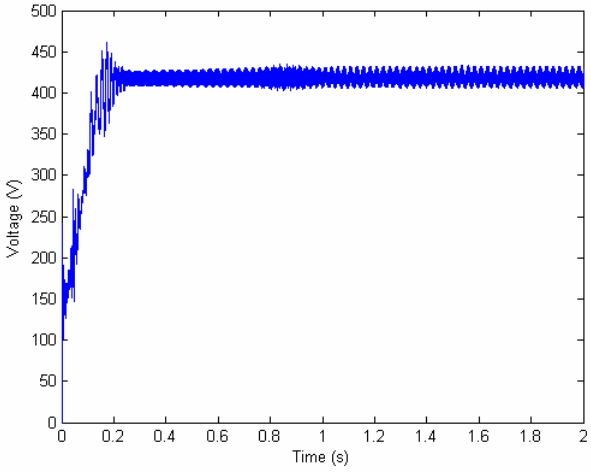

Fig. 15. DC bus voltage at startup for test-bed powered by the generator set.

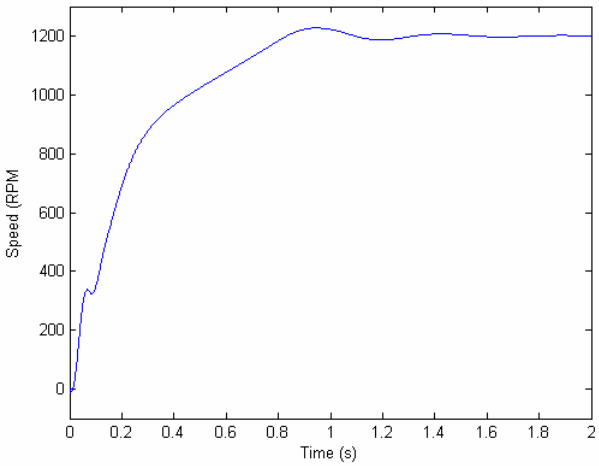

Fig. 16. Motor speed at startup for test-bed powered by the generator set.

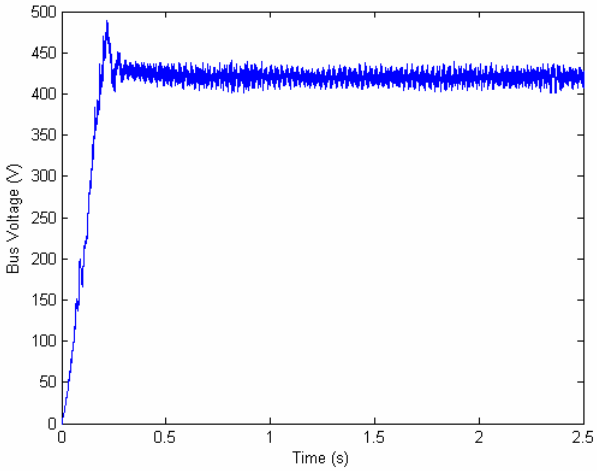

Fig. 17. DC bus voltage at startup for test-bed powered by the Li-Ion battery.

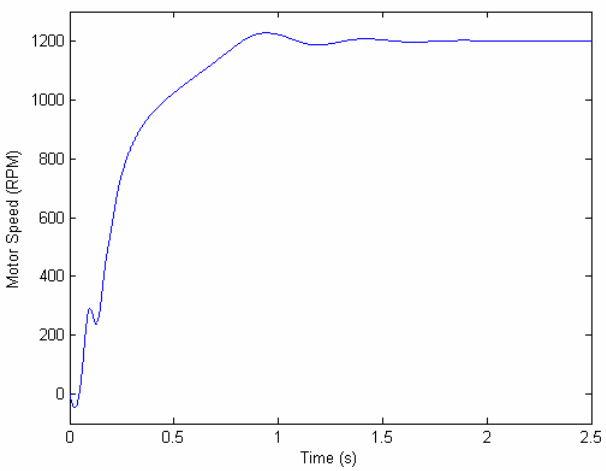

Fig. 18. Motor speed at startup for test-bed powerd by the Li-Ion battery.